phys. stat. sol. (b) **245**, No. 10, 1967–1970 (2008) / **DOI** 10.1002/pssb.200879569

physica status solidi b
www.pss-b.com
basic solid state physics

Electrochemical functionalization of SWNT bundles in acid and salt media as observed by Raman and X-ray photoelectron spectroscopy

Peter M. Rafailov[*,1], Christian Thomsen[2], Milko Monev[3], Urszula Dettlaff-Weglikowska[4], and Siegmar Roth[4]

[1] Georgi Nadjakov Institute of Solid State Physics, Bulgarian Academy of Sciences, 72 Tzarigradsko Chaussee blvd., 1784 Sofia, Bulgaria
[2] Institut für Festkörperphysik, Technische Universität Berlin, Hardenbergstr. 36, 10623 Berlin, Germany
[3] Acad. R. Kaishew Institute of Physical Chemistry, Bulgarian Academy of Sciences, 1113 Sofia, Bulgaria
[4] Max-Planck-Institut für Festkörperforschung, Heisenbergstr. 1, 70569 Stuttgart, Germany

Received 24 April 2008, revised 9 June 2008, accepted 10 June 2008
Published online 26 August 2008

PACS 63.22.Gh, 73.63.Fg, 78.30.Na, 81.07.De, 82.80.Pv, 82.45.Fk

[*] Corresponding author: e-mail rafailov@physik.tu-berlin.de, Phone: +359 2 979 5718, Fax: +359 2 975 36 32

We carried out electrochemical functionalization of single-walled carbon nanotube mats (buckypaper) in HCl and KCl aqueous solutions by exposing them to electrochemical potentials above the Cl^- oxidation potential and high Faradaic currents. Formation of C-Cl covalent bonds was established by X-ray Photoelectron Spectroscopy (XPS). Combining results from Raman, XPS and conductivity measurements, we find a significantly higher degree of covalent functionalization in the HCl solution as compared to the KCl one. We also discuss the impact of electrochemical doping and functionalization on the morphology and the conductivity of the SWNT sample.

1 Introduction The implementation of the extraordinary properties of carbon nanotubes into working devices is in many cases hindered by their insolubility and chemical inertness. One way to overcome this problem is functionalization of the nanotubes, i.e. attachment of appropriate chemical functionalities to a nanotube [1]. Nanotubes can thus be made selectively reactive with other compounds or soluble in certain solvents. Side-wall functional groups can react with polymers and improve the mechanical properties of nanocomposites [2]. Organic molecules can be coupled with functionalized nanotubes for sensor applications. Specific functionalization involving covalent bonds can create cross-links between SWNTs to form complex nanotube networks [1]. Functionalization can also be of great help for the development of large-scale separation techniques for metallic and semiconducting tubes, as most of the functionalization procedures are sensitive to the electronic properties of the SWNT [3].

Electrochemistry offers promising methods for functionalization based on the natural catalytic properties of electrolysis [4]. Electrochemical functionalization is especially convenient for nanotubes due to their large surface-to-volume ratio. On the other hand, quantum confinement effects render nanotubes extremely efficient in light scattering so that even modifications of the electronic structure of distinct nanotube chiralities (n,m) are observable by, e.g., Raman spectroscopy [5, 6]. Electrochemical functionalization can therefore be precisely controlled by conductance measurements [7] and monitored by Raman [8, 9], IR [9], or absorption [10] spectroscopy.

2 Experimental A stripe of SWNT "buckypaper" with a nanotube diameter distribution ranging from 1.25 nm to 1.45 nm and a surface density of about 10^{-5} g/mm^2 was prepared as a working electrode in a three-electrode cell equipped with quartz windows for *in situ* spectroscopic control. The measurements were carried out using a Metrohm Three-Electrode-Potentiostat. A platinum wire and Ag/AgCl/3 M KCl served as auxiliary and reference electrode, respectively. The working electrode was electri-

cally contacted at its end and was partly dipped into the solution. The electrolyte solution was purged with N_2 gas prior to the measurements to remove dissolved oxygen. All chemicals used were of analytical grade quality. The solutions were prepared using doubly distilled water.

The nanotube electrode was polarized anodically in order to utilize the relatively low oxidation potential of the chloride ions (1140 mV vs. Ag/AgCl). Oxidation of the OH^- ions on carbon electrodes in alkali choride solutions is normally shifted to higher potentials due to a high overvoltage. Hence possible electrolytic reactions at potentials of 1200–1500 mV comprise predominantly oxidation of Cl^- at the surface of the SWNT anode. Above 1200 mV a formation of gas bubbles commenced with increasing strength which caused large noise and suppressed the signal so it became impossible to proceed with the Raman monitoring above 1500 mV. The SWNTs were doped in the potentiostatic mode and Raman spectra were measured *in situ* at the end of each potential step after waiting for the cell current to decrease below 5 mA/g to ensure quasi-equilibrium conditions [11]. Due to the significant cell current flowing above 1000 mV, the exact determination of the applied potential was difficult, therefore from 1100 mV the cell was operated in galvanostatic mode, the corresponding constant current flowing through the cell for 20 minutes in each single experiment. To ensure connexity of the layout, potential values above 1100 mV are quoted as approximate estimates.

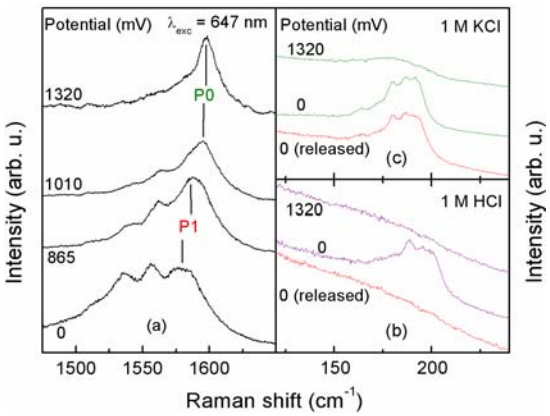

Figure 1 *Left*: Raman spectra at 1.92 eV excitation energy of the high-energy G-mode (a) showing intensity redistribution between the main peak P1 and a new peak P0 appearing at higher electrochemical potentials. Representative for both KCl and HCl solutions. *Right*: Raman spectra of the radial breathing mode in HCl (b) and in KCl (c) solution showing intensity redistribution and attenuation at high potentials.

The Ar^+Kr^+ laser line at 1.92 eV was used for excitation. The Raman spectra were recorded *in situ* with a DILOR triple-grating spectrometer equipped with a CCD detector. The spectrometer was calibrated in frequency using a Neon lamp and the laser plasma lines. After electrochemical processing the nanotube samples were rinsed in water and dried in an inert atmosphere. The conductivity measurements were performed by the four-probe method. The XPS measurements were carried out in the UHV-chamber of the electron spectrometer ESCALAB-MkII (VG Scientific Ltd.) with a base pressure of 10^{-8} Pa. The photoelecron spectra were excited with the Mg K_α radiation (1253.6 eV) with a total instrumental resolution of about 1 eV. The C 1s and Cl 2p photoelectron lines were recorded. All spectra were calibrated by using the C 1s line centered at 285 eV.

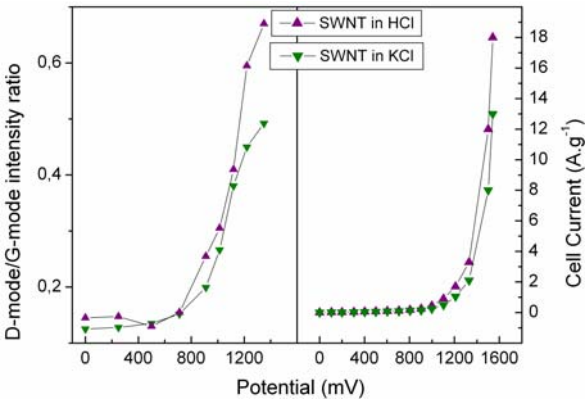

Figure 2 *Left*: Evolution of the D-mode/G-mode intensity ratio as a function of the applied potential in HCl and in KCl solution. *Right*: Specific current flowing through the electrochemical cell vs the applied potential. At higher potentials above 1100 mV the cell was operated in galvanostatic mode.

3 Results and discussion Electrochemical processing results in a dramatic intensity redistribution in both the high-energy mode (HEM) and the radial breathing mode (RBM) and a strong attenuation of the RBM in the Raman spectra of SWNTs at high electrochemical potentials (see Fig. 1). The appearance of the new peak P0 in the HEM [12] and the almost complete intensity loss of the RBM point to a principle change in the doping mechanism from double-layer charging at the outer surface of the SWNT bundles to a massive penetration of the bundles by chlorine species upon crossing the Cl^- oxidation potential as indicated also by the strong current increase (Fig. 2). Via ionic bonding these chlorine species can cause a much stronger p-doping than the preceding double-layer doping at low potentials, resulting in a depletion of the van Hove singularities responsible for the Raman resonance. On the other hand, functionalization via C-Cl covalent bonding leads to a local disruption of the delocalized electronic structure based on the sp^2-bonded network of the SWNTs. Therefore, both ionic and covalent functionalization lead to a loss of resonance and can account for the strong attenuation of the RBM band [3]. Additionally, the penetration into the SWNT bundles suppresses the intertube van der Waals interaction which to a considerable extent governs the RBM vibrational motion [13].

Table 1 Contents of chlorine (in at%), ionically and covalently bonded to the nanotube walls depending on the experimental conditions (electrolyte type and applied potential).

Experimental conditions	Contents (in at%)	
	Covalently bonded	Ionically bonded
1150 mV, HCl	1.2	0.5
1150 mV, KCl	0.8	1.9
1400 mV, HCl	2.5	0.6
1400 mV, KCl	1.7	2.6

The sharp increase of the D/G mode intensity ratio presented in Fig. 2 and the XPS evidence in Fig. 3 (red shift of the C 1s photoelectron peak and increasing intensity of the Cl 2p doublet with 3/2-component centered at 200.2 eV), indicate an increasing share of chlorine atoms covalently bonded to the nanotube walls [1, 14, 15]. This increase is, however, more strongly pronounced in the HCl solution, where covalent bonding becomes the main functionalization type. In the KCl solution, as depicted in Fig. 3, ionic bonding prevails and covalent functionalization increases only slowly with electrochemical potential. This is consistent with the observation that in the KCl solution the RBM could be almost completely recovered upon releasing potential back to 0 mV (see Fig. 1) while the RBM was irrecoverably lost after processing at high potentials and currents in the HCl solution. The contents of chlorine ionically and covalently bonded to the nanotubes as calculated from the XPS analysis, are summarized in Table 1.

The SWNT sample processed at ≈ 1400 mV in 1M KCl was additionally tested by energy-dispersive X-ray analysis (EDAX) which revealed a potassium content of 1.1 weight % and a Cl content of 13.2 weight %. Assuming some residual quantity of crystallized KCl in the pores of the SWNT mat, it turns out that ≈ 12 weight % of the Cl content correspond to adsorbed and covalently bonded chlorine. This quantity is roughly equal to the 4.3 atomic

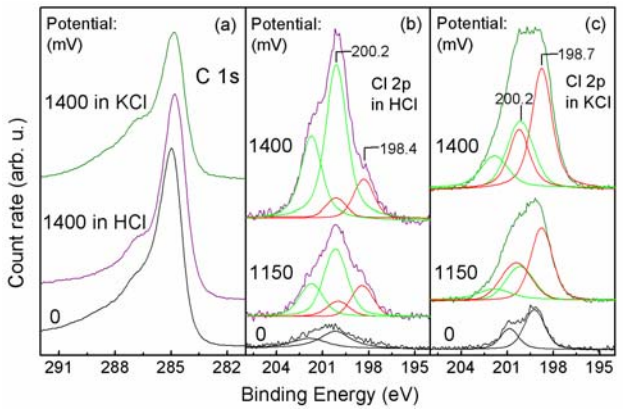

Figure 3 X-ray photoelectron spectra of carbon 1s (a), and chlorine 2p from SWNT samples polarized to different maximal potentials in 1 M solutions of HCl (b) and KCl (c) as quoted in the graphs. Potential = 0 mV means pristine sample.

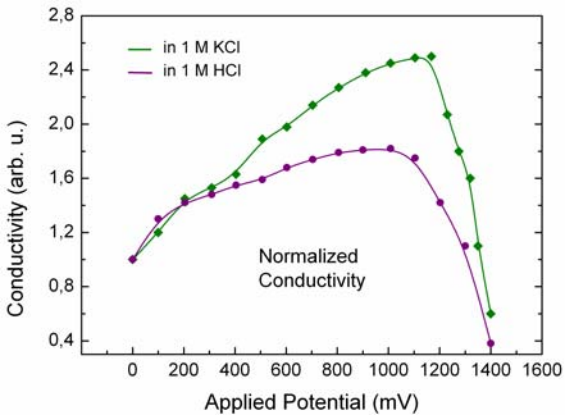

Figure 4 DC conductivity of the SWNT working electrode vs maximal applied potential in KCl and in HCl solution. The displayed values are normalized to the conductivity of the undoped sample.

% of total chlorine content calculated from the last row of Table 1. The reliability of the values given in Table 1 was thus additionally confirmed by EDAX.

The SWNT conductivity is enhanced by double-layer charging and physisorption of chlorine species and is subsequently suppressed by covalent functionalization of the nanotube walls, as depicted in Fig. 4, because formation of covalent bonds leads to a localization of the nanotube electronic states thus lowering the concentration of free carriers. Again, the steeper conductivity drop in the HCl solution shows a higher degree of covalent functionalization. The penetration of electrolyte species into the interstitial channels of SWNT bundles may cause partial disintegration of the bundles thus further lowering the conductivity by reducing the metallic percolation paths within the bundles [16].

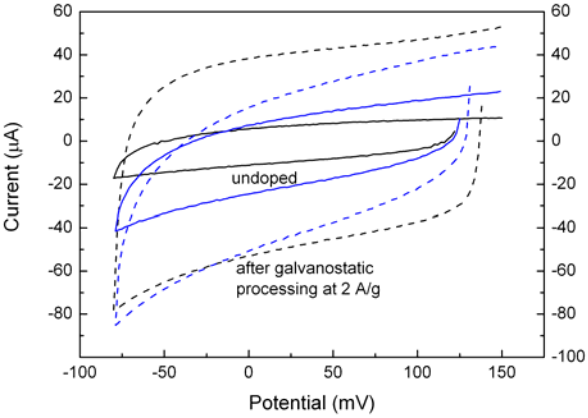

Figure 5 Cyclic voltammograms (CVA) of the SWNT working electrode in 1 M KCl (black traces) and 1 M HCl (blue traces). The CVAs plotted with solid lines correspond to the undoped samples while those plotted with dashed lines were obtained after galvanostatic processing of the samples at a current of 2 A/g.

To check the assumption for bundle penetration we examined the effective surface area of our samples by cyclic voltammetry. Cyclic voltammograms (CVA) were measured before doping and after galvanostatic processing at a specific current of 2 A/g which roughly corresponds to potential values between 1200 and 1400 mV. The results are displayed in Fig. 5. A CVA comprises the cyclic charging/discharging process of the double layer at the working electrode, therefore its saddle-point current is proportional to the effective surface area (ESA) of the electrode [17]. As can be appreciated from Fig. 5, this galvanostatic processing of the SWNT buckypaper brings about a fivefold increase of the ESA in the KCl solution and a more than twofold increase of the ESA in the HCl one. This can only be understood if one assumes that the interior of the SWNT bundles becomes largely accessible for the electrolyte ions, i.e., either the interstitial channels become larger, or the bundles disintegrate into smaller ones. On the other hand, the higher current for the undoped sample cycled in the HCl solution indicates some initial penetration into the SWNT bundles in acid environment even in very narrow potential ranges essentially free of faradaic processes.

4 Conclusions We were able to electrochemically functionalize a mat of SWNT bundles by using it as working electrode in chloride solutions with anodic polarization above the oxidation potential of Cl^-. The degree of covalent functionalization achieved is significantly higher in the HCl solution as compared to the KCl one. On the other hand, non-covalent functionalization prevails when processing the SWNT electrode in a KCl solution. Formation of scattering centers through covalent bonding and a partial de-bundling of the SWNTs, for which we obtained consistent evidence from Raman, conductivity and cyclic-voltammetry measurements, lead to a steep drop in the sample conductivity due to vanishing metallic percolation paths within the bundles.

Acknowledgements P.M.R. acknowledges support from the NATO Reintegration Grant Nr. CBP.EAP.RIG.982322.

References

[1] U. Dettlaff-Weglikowska, J.-M. Benoit, P.-W. Chiu, R. Graupner, S. Lebedkin, and S. Roth, Curr. Appl. Phys. **2**, 497 (2002).
[2] C. A. Dyke and J. M. Tour, J. Phys. Chem. A **108**, 11151 (2004).
[3] R. Graupner, J. Raman Spectrosc. **38**, 673 (2007).
[4] E. Unger, A. Graham, F. Kreupl, M. Liebau, and W. Hoenlein, Curr. Appl. Phys. **2**, 107 (2002).
[5] L. Kavan, M. Kalbáč, M. Zukalová, and L. Dunsch, J. Phys. Chem. B **109**, 19613 (2005).
[6] L. Kavan, M. Kalbáč, M. Zukalová, and L. Dunsch, phys. stat. sol. (b) **243**, 3130 (2006).
[7] B. R. Goldsmith, J. G. Coroneus, V. R. Khalap, A. A. Kane, G. A. Weiss, and P. G. Collins, Science **315**, 77 (2007).
[8] J. L. Bahr, J. Yang, D. V. Kosynkin, M. J. Bronikowski, R. E. Smalley, and J. M. Tour, J. Am. Chem. Soc. **123**, 6536 (2001).
[9] P. M. Rafailov, C. Thomsen, U. Dettlaff-Weglikowska, and S. Roth, J. Phys. Chem. B, in print.
[10] M. S. Strano, C. A. Dyke, M. L. Usrey, P. W. Barone, M. J. Allen, H. Shan, C. Kittrell, R. H. Hauge, J. M. Tour, and R. E. Smalley, Science **301**, 1519 (2003).
[11] A. Claye, S. Rahman, J. E. Fischer, A. Sirenko, G. U. Sumanasekera, and P. C. Eklund, Chem. Phys. Lett. **333**, 16 (2001).
[12] P. M. Rafailov, J. Maultzsch, C. Thomsen, and H. Kataura, Phys. Rev. B **72**, 045411 (2005).
[13] C. Thomsen, S. Reich, A. R. Goni, H. Jantoljak, P. M. Rafailov, I. Loa, K. Syassen, C. Journet, and P. Bernier, phys. stat. sol. (b) **215**, 435 (1999).
[14] G. S. Duesberg, R. Graupner, P. Downes, A. Minett, L. Ley, S. Roth and N. Nicoloso, Synth. Met. **142**, 263 (2004).
[15] U. Dettlaff-Weglikowska, V. Skakalova, R. Graupner, S. H. Jhang, B. H. Kim, H. J. Lee, L. Ley, Y. W. Park, S. Berber, D. Tomanek, and S. Roth, J. Am. Chem. Soc. **127**, 5125 (2005).
[16] V. Skakalova, A. B. Kaiser, Y.-S. Woo, and S. Roth, Phys. Rev. B **74**, 085403 (2006).
[17] M. Stoll, P. M. Rafailov, W. Frenzel, and C. Thomsen, Chem. Phys. Lett. **375**, 625 (2003).

